J Mater Sci (2011) 46:5071–5078
DOI 10.1007/s10853-011-5433-8

The effects of electronic structure of non-metallic doped TiO_2 anode and co-sensitization on the performance of dye-sensitized solar cells

Xin Zheng · Jingchang Zhang · Lingli Peng · Xiuying Yang · Weiliang Cao

Received: 3 December 2010 / Accepted: 2 March 2011 / Published online: 10 March 2011

Abstract N/TiO_2, S/TiO_2, and $N\ S/TiO_2$ nanocrystalline films anode were obtained by doping non-metallic element N and S which could change the LUMO of anode, leading to the easy injection of electron from the excited state of dye molecule to the conduction band of semiconductor, and thus improving the photoelectric conversion efficiency and reducing the impedance of solar cells. The anode films treated by titanium tetrachloride and co-sensitized by P3HT/N719 were also studied. The absorption region of P3HT/N719 covered the entire visible region in the solar cells. The solar cell based on N/TiO_2 anode film treated by titanium tetrachloride and P3HT/N719 showed a short-circuit current density of 10.20 mA/cm^2, open-circuit voltage of 0.557 V, and photoelectric conversion efficiency of 2.55%.

Introduction

Dye-sensitized solar cells (DSSCs) have attracted much attention for their high efficiency, low-cost, and flexible choices in varied and fine-tuned materials since Grätzel and O'Regan first reported the DSSCs in 1991 [1, 2].

The most extensive studies on DSSCs [3, 4] were based on the material of TiO_2, which has a wide bandgap semiconductor, and the rutile and the anatase phases. TiO_2 can only absorb UV light under 387 nm, leading to the lower utilization of solar energy [5, 6]. There are also some reports about doped TiO_2 nanomaterials with metal elements [7–10]. However, there has been no report about the energy level match between the LUMO of the anode's doped with non-metallic element and the electronic structure of the dye.

In this article, TiO_2 was doped with N and S to reduce the LUMO level of TiO_2, leading to the easy injection of electron from the excited state of dye molecule to the conduction band of TiO_2, and the improvement of the conversion efficiency of solar cells. Moreover, we found that there is a threshold for the LUMO of the TiO_2 anode doped by N and S. The too low LUMO can result in the annihilation of the excited electrons in the semiconductor conduction band with the oxidation state dye. In addition, the solar cell co-sensitized by P3HT/N719 supplied a higher efficiency than single-sensitization cells because P3HT/N719 covered the entire visible region. Notable, the study of improving the DSSCs conversion efficiency by two dyes (P3HT/N719) has not been reported.

Experimental

Preparation of nano-TiO_2 powder by hydrothermal method

The nano-TiO_2 powder was prepared with $TiCl_4$ solution as the raw material according to reference [11].

TiO_2 (0.01 g) was dissolved in isopropyl alcohol (2 mL) and dropped evenly on a clean quartz glass and ITO conductive glass. White TiO_2 films were obtained on vacuum drying the glass.

X. Zheng · J. Zhang · L. Peng · W. Cao
State Key Laboratory of Chemical Resource Engineering, Institute of Modern Catalysis, Beijing University of Chemical Technology, Beijing 100029, China

J. Zhang (✉) · X. Yang · W. Cao
Hainan Institute of Science and Technology, Haikou 571126, China
e-mail: zhangjc1@mail.buct.edu.cn

Preparation of nano-N/TiO_2, nano-S/TiO_2, and nano-N S/TiO_2 powders by hydrothermal method

Surfactant polyethylene glycol (PEG 800) was added to 0.3 mol/L of $TiCl_4$, followed by stirring vigorously at ambient temperature. The pH of the solution was adjusted to 5–6 by dripping ammonia. The sol was filtered and washed with ammonia until no presence of Cl^-, and then transferred into a PTFE autoclave (100 mL) and maintained at 240 °C for 12 h. Then the sol was washed by ethanol until no water existed. The obtained alcogel was dried at room temperature, and calcined at 500 °C for 1 h to give the nano-N/TiO_2.

The TiO_2 nano-powder prepared in "Preparation of nano-TiO_2 powder by hydrothermal method" section was soaked in 1 mol/L sulfuric acid solution with the molar ratio 2:1 for 12 h. After calcination at 500 °C for 1 h, the powder of nano-S/TiO_2 was finally prepared.

The N/TiO_2 nano-powder prepared was soaked in 1 mol/L thiourea solution with the molar ratio 2:1 for 12 h. After calcination at 500 °C for 1 h, the powder of nano-N S/TiO_2 was finally prepared.

N/TiO_2 (0.01 g), S/TiO_2 (0.01 g), and N S/TiO_2 (0.01 g) were, respectively, suspended in isopropyl alcohol (2 mL) and dropped evenly on clean quartz glasses and ITO. White N/TiO_2, S/TiO_2, and N S/TiO_2 films were obtained after drying in vacuum.

Synthesis of poly(3-hexylthiophene)

Poly(3-hexylthiophene) was synthesized according to the literature [12]. 3-hexylthiophene monomer and chloroform were added to a 100-mL flask and ultrasonically dispersed for 15 min. The temperature of system was controlled at 0 °C. $FeCl_3$ was dissolved in chloroform, and added dropwise to the flask. The reaction mixture was stirred under high-purity nitrogen for 8 h. The product was slowly added to methanol, precipitated, filtered, and subjected to Soxhlet extraction with methanol for 20 h. The P3HT was then dried under vacuum at room temperature.

Preparation of DSSCs

Preparation of TiO_2 films, N/TiO_2 films, S/TiO_2 films, and N S/TiO_2 films by combination technique

$TiCl_4$ sol was dropped on the clean FTO glass substrate using spinning at the rate of 3000 r/min for 20 s. TiO_2 (0.01 g), N/TiO_2 (0.01 g), S/TiO_2 (0.01 g), and N S/TiO_2 (0.01 g) were, respectively, suspended in ethanol (2 mL), and dropped evenly on the above FTO substrate by spin coating at the rate of 3000 r/min for 20 s. After the drying at room temperature and calcination at 450 °C for 30 min, TiO_2, N/TiO_2, S/TiO_2, and N S/TiO_2 anodes were prepared.

N/TiO_2 anode films treated by titanium tetrachloride

N/TiO_2 anode films prepared in "Preparation of TiO_2 films, N/TiO_2 films, S/TiO_2 films, and N S/TiO_2 films by combination technique" section were impregnated with 0.1 mol/L of $TiCl_4$ aqueous solution in a closed chamber at 65 °C for 20 min, washed with deionized water, fully rinsed with ethanol, and finally heated at 450 °C for 30 min [13].

Preparation of Pt electrode

H_2PtCl_6 was evenly dropped on another FTO substrate, dried at 25 °C, and calcined at 380 °C for 30 min to prepare Pt electrode.

Sensitization and pack of anode

TiO_2, N/TiO_2, S/TiO_2, and N S/TiO_2 anode thin films prepared in "Preparation of TiO_2 films, N/TiO_2 films, S/TiO_2 films, and N S/TiO_2 films by combination technique" section were soaked in N719 (5 mmol/L in chloroform) at 80 °C for 12 h. N/TiO_2 anode thin film was soaked in N719/P3HT (the mixture of 5 mmol/L P3HT in chloroform and 5 mmol/L N719 in ethanol with the volume ratio 1:2) at 80 °C for 12 h. N/TiO_2 anode thin films treated by titanium tetrachloride soaked, respectively in N719 and N719/P3HT at 80 °C for 12 h. Dye attached in the surface layer was washed with anhydrous ethanol, and dried at 80 °C for 15 min to prepare the sensitized anode thin films. DSSCs were obtained after the package by using Pt electrode with epoxy resin film, the injection of electrolyte, and seal.

Structural characterization

X-ray diffraction

X-ray diffraction (XRD) measurements were performed using a Shimadzu HR6000X (Cu target X tube, voltage 40.0 kV, current 30.0 mA) to test the powder sample. The average particle size can be calculated by using the Scherrer formula.

Transmission electron microscope

Transmission electron microscope (TEM) measurements were performed on a HITACHI-800.

X-ray photoelectron spectroscopy

X-ray photoelectron spectroscopy (XPS) analyses were conducted by ESCALAB 250.

Performance characterization

UV–Vis spectra

UV–Vis spectra were measured using Hitachi U-3010 spectrophotometer.

Cyclic voltammetry

Cyclic voltammetry (CV) measurements were carried out with the Potentiostiostat/Galvanostat (EG&G PAR Model 283). The counter electrode was platinum and the reference electrode was non-aqueous Ag/Ag^+. The CV curves were recorded in acetonitrile with 0.1 mol/L $LiClO_4$ at a scanning rate of 50 mV/s. The $LiClO_4$ solution was insufflated with N_2 for 30 min before use. E_{HOMO}, E_{LUMO}, and E_g were calculated by using the formula as follows [14, 15]:

$$E_{HOMO}(\text{or } E_{LUMO}) = E_0 + eV_{ox}(\text{or } eV_{red}) \quad (1)$$

$$E_g = E_{LUMO} - E_{HOMO} \quad (2)$$

E_{HOMO} is the electrode potential of the highest occupied molecular orbital, E_{LUMO} is the electrode potential of the lowest unoccupied molecular orbital, E_0 is the standard electrode potential (−4.4 eV) of Ag/Ag^+ electrodes. φ_{ox} is the oxidation potentials of electrode (as opposed to Ag/Ag^+ electrodes). φ_{red} is the redox potentials of electrode (as opposed to Ag/Ag^+ electrodes).

Current–voltage (I–V)

Current–voltage (I–V) were recorded in air at room temperature (298 K) using a Keithley 236 high current source powder meter under white-light illumination from a 500 W xenon lamp. The light intensity was about 100 mW/cm^2 on the sample surfaces measured by a photodetector. To measure the decay, the short-circuit current (J_{sc}) and open-circuit voltage (V_{oc}) as a function of the illumination time were recorded. Electrochemical Impedance Spectroscopy (EIS) measurements were carried out at the Potentiostiostat/Galvanostat (EG&GPARModel283). The measured frequency was range of 50 mHz–100 kHz.

Results and discussion

XRD Characterization of TiO_2, N/TiO_2, S/TiO_2, and N S/TiO_2

The XRD patterns for the TiO_2, N/TiO_2, S/TiO_2, and N S/TiO_2 powders are shown in Fig. 1. In XRD patterns of TiO_2, the peaks at 25.32°, 37.80°, 48.11°, 54.02°, 55.18°, and 62.72° are assigned to the (101), (004), (200), (105), (211), and (213) lattice planes [16, 17], which are attributed to the signals of the anatase phase. There is no N and S diffraction peaks in the XRD spectra, indicating doping elements dispersed in TiO_2 with a high degree form. It can be calculated that the average TiO_2, N/TiO_2, S/TiO_2, and N S/TiO_2 particles are 22.22, 13.69, 12.61, and 10.79 nm, respectively by Scherrer formula. These results indicate doping non-metallic elements can significantly inhibit the growth and increase the specific surface area of nano-TiO_2 grains, which is very helpful for the adsorption of dyes on TiO_2, N/TiO_2, S/TiO_2, and N S/TiO_2 electrodes.

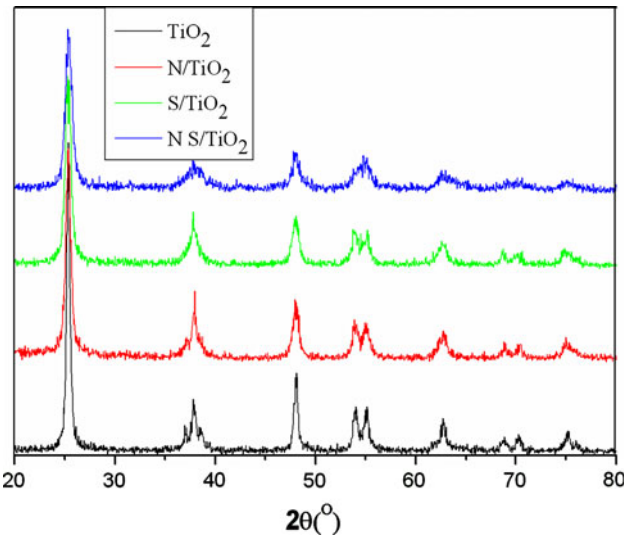

Fig. 1 XRD patterns for the TiO_2, N/TiO_2, S/TiO_2, and N S/TiO_2 powders

TEM measurements of TiO_2, N/TiO_2, S/TiO_2, and N S/TiO_2

Figure 2a–d demonstrate TEM results of TiO_2, N/TiO_2, S/TiO_2, and N S/TiO_2. From the TEMs, the powder particles have approximate spherical and uniform size, and disperse well. TiO_2 size is 22–24 nm, both N/TiO_2 and S/TiO_2 size are 12–14 nm, and N S/TiO size is 10–12 nm. The results are almost the same with the Scherer formula. Alcohol exchange in the powder preparation eliminated the liquid surface tension and reduced agglomeration of particles in the calcining process. Therefore, nano-particles with high surface area, small size, and good dispersion were obtained.

XPS characterization of N/TiO_2

Figure 3a–c is the high-resolution XPS of N/TiO_2. In the N/TiO_2 sample (Fig. 3a), the XPS shows Ti, O, N, and C signals, and Cl was not obvious in the sample. Figure 3b shows that the narrow scans for Ti2p peaks locate at

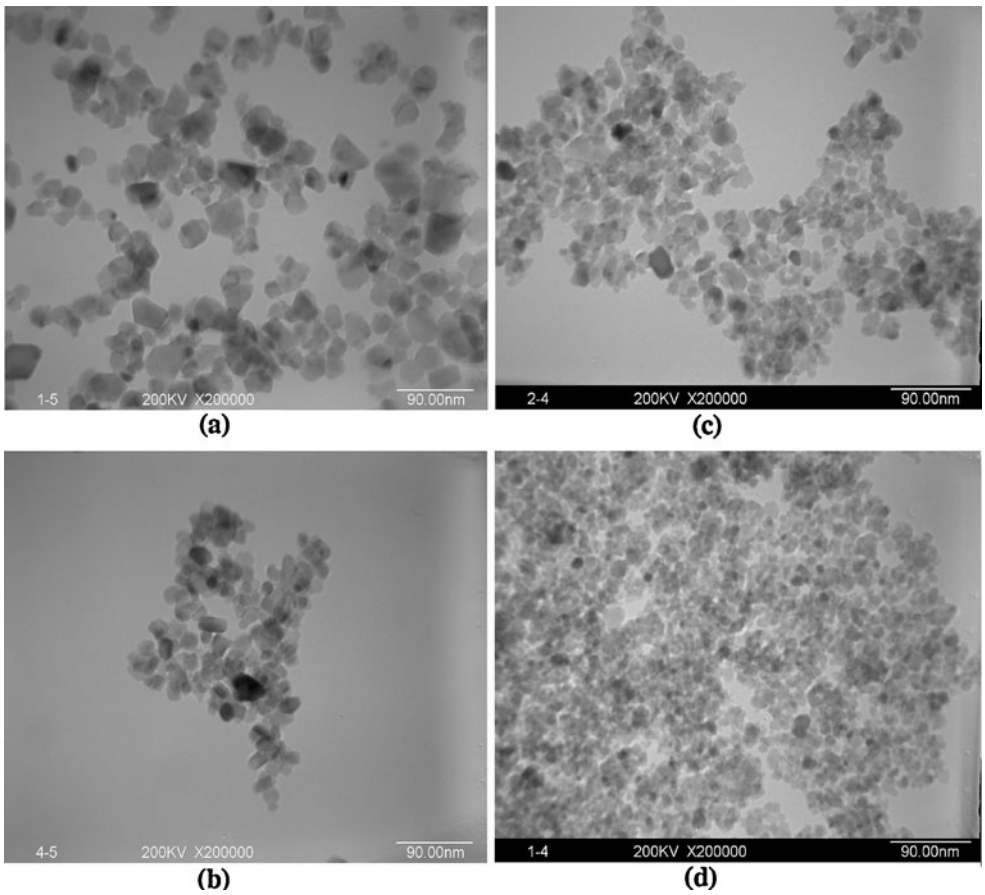

Fig. 2 TEM patterns of **a** TiO_2, **b** N/TiO_2, **c** S/TiO_2, and **d** $N\ S/TiO_2$ powders

464.12 eV (Ti $2p_{1/2}$) and 458.34 eV (Ti $2p_{3/2}$) for N/TiO_2. Compared with TiO_2, a high binding energy-shift has taken place. The electric binding energy of the N1s in the N/TiO_2 sample locates at 399.90 eV. N doped into the TiO_2 lattice could form Ti–N, which resulted in the change of the electron density around Ti and the electric binding energy of N. Therefore, the N doping is the replacement rather than the simple adsorption [18].

UV–Vis spectra of TiO_2, N/TiO_2, S/TiO_2, $N\ S/TiO_2$, and dye

The UV–Vis spectra of TiO_2, N/TiO_2, S/TiO_2, and $N\ S/TiO_2$ nanocrystalline thin film electrodes prepared by combination technology are shown in Fig. 4. All of the absorption peaks of N/TiO_2, S/TiO_2, and $N\ S/TiO_2$ nanocrystalline thin film electrodes have a red-shift.

The UV–Vis spectra of N719 and P3HT films are shown in Fig. 5. From the spectrum of N719 film, there were three absorption bands with maximum wavelength of 320, 400, and 550 nm, and the absorption covered the entire range of UV–Visible. There was only one absorption band for P3HT film with the maximum wavelength of 500 nm. The spectra of the P3HT and N719 are so complementary that the absorption of P3HT/N719 can cover the full visible light. The full cover can improve the photoelectric conversion efficiency of solar cells.

Cyclic voltammetry

CV curves of TiO_2, N/TiO_2, S/TiO_2, and $N\ S/TiO_2$ nanocrystalline thin film electrodes prepared by combination technology are shown in Fig. 6. P3HT, N719, and N719/P3HT thin films CV curves are shown in Fig. 7. The frontier orbital and energy gap of TiO_2, N/TiO_2, S/TiO_2, and $N\ S/TiO_2$, P3HT, N719, and N719/P3HT thin films are listed in Table 1. According to data in Table 1, Fig. 8 was obtained. The energy gap of pure anatase TiO_2 is 3.18 eV. Non-metallic element doping led to a significant reduce for the energy gap, which is the same with UV–Vis spectra. Process (1) in Fig. 8 shows the transition of electrons from the ground state of dye molecules (D) to the excited state (D*) when excited by light ($D + h\nu \rightarrow D^*$). Process (2) shows that the excited electrons injected into the semiconductor conduction band ($D^* \rightarrow D^+ + e^-$). Process (3) indicates the complex of the electrons between

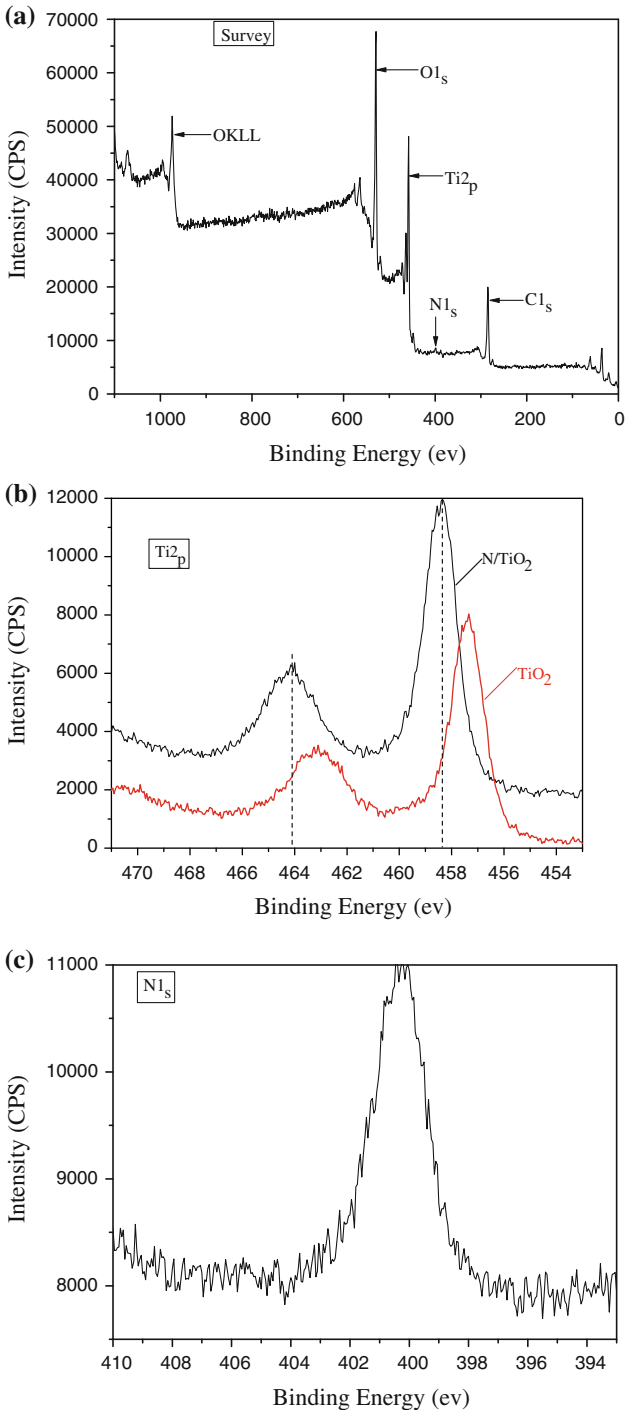

Fig. 3 XPS spectra of N/TiO_2 powders

semiconductor conduction band and oxidation state dye ($D^+ + e^- \rightarrow D$). Process (4) represents that the electrons transfers from the semiconductor to the conductive glass [19]. According to Process (2), when the LUMO level of dye molecule is superior to the LUMO level of semiconductor, the electrons could transfer to the semiconductor conduction band. In addition, because of Process (3) which can reduce the current, the LUMO of semiconductor and

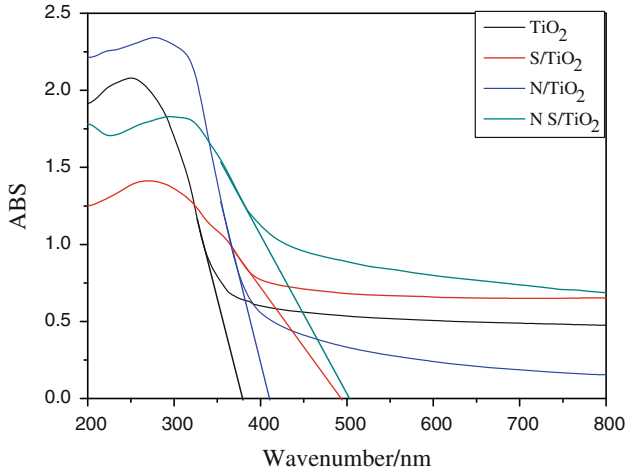

Fig. 4 UV–Vis spectras of TiO_2, N/TiO_2, S/TiO_2, and N S/TiO_2 nanocrystalline thin film electrodes

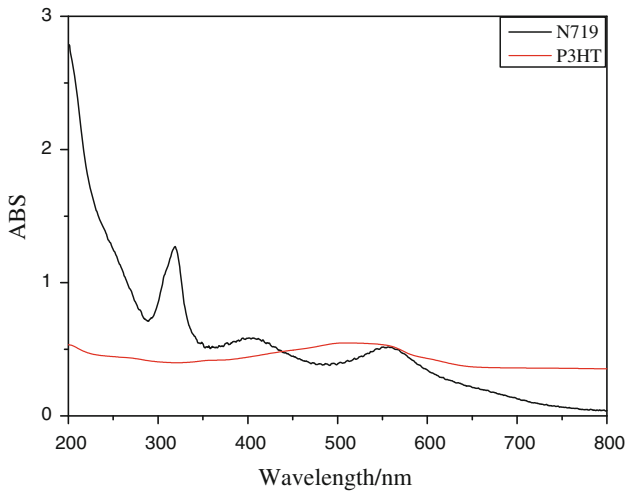

Fig. 5 UV–Vis spectras of N719 and P3HT films

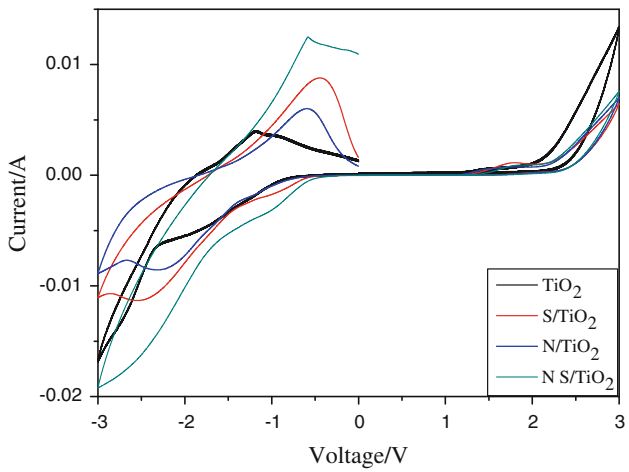

Fig. 6 CV curves of TiO_2, N/TiO_2, S/TiO_2, and N S/TiO_2 nanocrystalline thin film electrodes

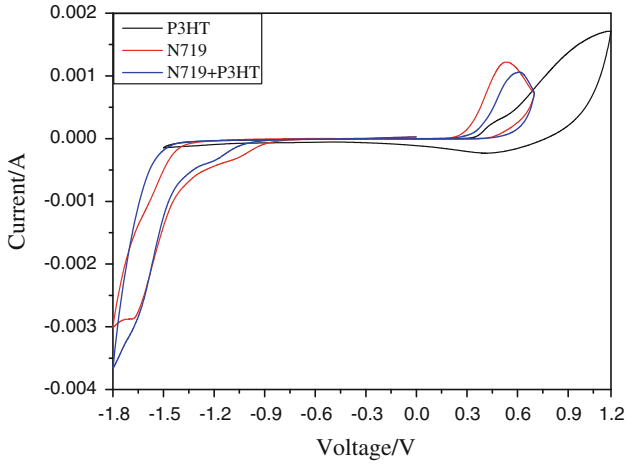

Fig. 7 CV curves of P3HT, N719, and N719/P3HT thin film

Table 1 The frontier orbital and energy gap of TiO_2, N/TiO_2, S/TiO_2, and N S/TiO_2, P3HT, N719, and N719/P3HT thin films

Sample	Φ_{ox} (eV)	Φ_{red} (eV)	E_{LUMO} (eV)	E_{HOMO} (eV)	E_g (eV)
TiO_2	2.15	−1.03	−3.41	−6.59	3.18
S/TiO_2	2.14	−0.52	−3.92	−6.58	2.66
N/TiO_2	2.15	−0.75	−3.69	−6.59	2.90
N S/TiO_2	2.14	−0.56	−3.88	−6.58	2.70
P3HT	0.47	−0.63	−3.81	−4.91	1.10
N719	0.30	−1.33	−3.11	−4.74	1.63
N719 + P3HT	0.36	−1.36	−3.08	−4.80	1.72

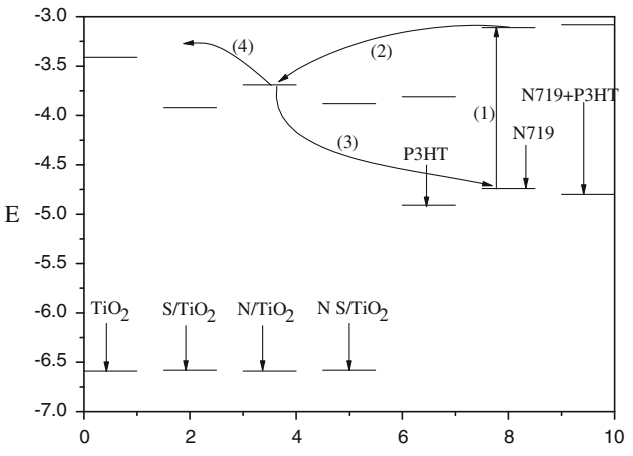

Fig. 8 Level matching condition of four different powders and three different dyes

the HOMO and LUMO of dye must match well. From Fig. 8, it can be seen that TiO_2, N/TiO_2, S/TiO_2, and N S/TiO_2 match well with the dye N719. Compared with N719, The LUMO became higher and the HOMO became lower after the mixing of N719 with P3HT. The change can

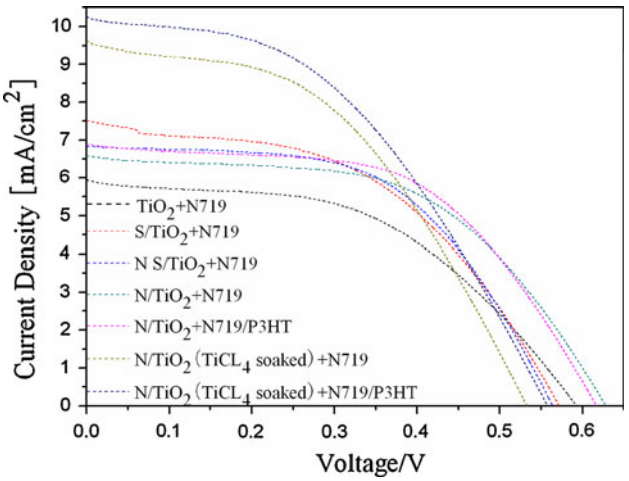

Fig. 9 Photochemical study of DSSCs

Table 2 Performance parameters of DSSCs

Cells	V_{oc} (V)	J_{sc} (mA/cm^2)	FF	η (%)
TiO_2 + N719	0.592	5.94	0.495	1.74
S/TiO_2 + N719	0.571	7.50	0.482	2.08
N S/TiO_2 + N719	0.563	6.83	0.555	2.13
N/TiO_2 + N719	0.628	6.57	0.543	2.24
N/TiO_2 + N719/P3HT	0.616	6.88	0.552	2.34
N/TiO_2($TiCl_4$ soaked) + N719	0.532	9.60	0.460	2.35
N/TiO_2($TiCl_4$ soaked) + N719/P3HT	0.557	10.20	0.448	2.55
N/TiO_2 + P3HT	0.420	0.94	0.444	0.18

enhance the injection of electron from excited state dye to the semiconductor conduction band, and also inhibit the complex between the electron in semiconductor conduction band and the oxidation state dye.

Performance parameters of DSSCs

The photovoltaic performances of the devices are shown in Fig. 9 and all the parameters of solar cells are listed in Table 2. N/TiO_2, S/TiO_2, and N S/TiO_2 solar cells sensitized by N719 performed better than the TiO_2 solar cell, and the N/TiO_2 solar cell was the best one. It gave a short-circuit current (J_{sc}) of 6.57 mA/cm^2, open-circuit voltage (V_{oc}) of 0.628 V, and an overall conversion efficiency (η) of 2.24%. This is mainly due to the lower energy gap after doping, and the better match of N/TiO_2 with N719. N/TiO_2 solar cell sensitized by N719/P3HT gave a short-circuit current (J_{sc}) of 6.88 mA/cm^2, an open-circuit voltage (V_{oc}) of 0.616 V, and an overall conversion efficiency (η) of 2.34%. Compared with N/TiO_2 only sensitized by N719, the result was mainly due to that the absorption ability of N719/P3HT covers the entire visible region. N/TiO_2 anode

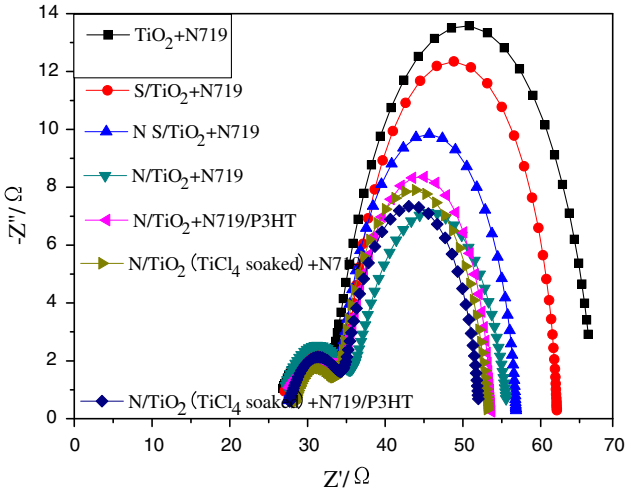

Fig. 10 EIS spectrums of DSSCs

Table 3 Impedance values of different parts of solar cells

Cells	R_s (Ω)	R_1 (Ω)	R_2 (Ω)
TiO_2 + N719	25.65	10.67	33.03
S/TiO_2 + N719	26.13	9.57	29.85
N S/TiO_2 + N719	26.44	9.15	25.47
N/TiO_2 + N719	26.95	9.08	23.83
N/TiO_2 + N719/P3HT	27.03	9.11	21.85
N/TiO_2($TiCl_4$ soaked) + N719	27.34	8.76	20.45
N/TiO_2($TiCl_4$ soaked) + N719/P3HT	27.64	8.84	19.66

films treated by titanium tetrachloride and then sensitized, respectively by N719 and N719/P3HT gave a short-circuit current (J_{sc}) of 9.60 and 10.20 mA/cm^2. The significant increases of short-circuit current were mainly due to that the electric contact was greatly improved after being treated by titanium tetrachloride [13].

EIS of DSSCs

EIS spectra of DSSCs are shown in Fig. 10 and all the impedance values of different parts of solar cells are listed in Table 3. R_s signifies the resistance of conductive glass FTO and transparent conductive film, R_1 signifies the interface charge transfer resistance between electrolyte and Pt electrode, and R_2 signifies the interface charge transfer resistance between electrolyte and TiO_2/dye [20, 21]. From Fig. 10 and Table 3, it can be found that there is little difference on R_s and R_1 for all the cells, while R_2 of N/TiO_2 sensitized by N719 is smaller than those of TiO_2, S/TiO_2 and N S/TiO_2 sensitized by N719, indicating that N/TiO_2 match better with N719 than TiO_2, S/TiO_2, and N S/TiO_2. R_2 of N/TiO_2 treated by titanium tetrachloride sensitized by N719 is smaller than that of N/TiO_2 sensitized by N719, indicating that the internal resistance can be largely reduced after treated by titanium tetrachloride. R_2 of N/TiO_2 treated by titanium tetrachloride sensitized by N719/P3HT is the smallest of all solar cells, which is consistent with the result in "Performance parameters of DSSCs" section.

Conclusions

(1) XRD, TEM, and XPS results show that N/TiO_2, S/TiO_2, and N S/TiO_2 were successfully doped with N and S. N/TiO_2, S/TiO_2, and N S/TiO_2 powders are anatase, and the average particle size distributed between 10 and 14 nm. N and S doping inhibited the growth of the particle size.

(2) CV, IV, and EIS tests show that the LUMO levels of N/TiO_2, S/TiO_2, and N S/TiO_2 are lower than that of TiO_2, which is helpful for the injection of electron from excited dye molecules to the semiconductor conduction band, and improves the photovoltaic conversion efficiency. However, the LUMO level has a threshold and must be appropriate because a too low LUMO would be beneficial for the complex between electron in the semiconductor conduction band and oxidation state dye. The LUMO level of N/TiO_2 matched best with N719/P3HT in the article.

(3) The solar cell with N/TiO_2 anode film treated by titanium tetrachloride and then sensitized by N719/P3HT had the highest conversion efficiency (η) of 2.55%, and it gave a short-circuit current (J_{sc}) of 10.20 mA/cm^2, and an open-circuit voltage (V_{oc}) of 0.557 V.

Acknowledgements The study was supported by the Key Planned Science and Technology Project of Hainan Province (ZDXM 20100062), the National High Technology Research and Development Program of Hainan under Grant no. 509013, the National High Technology Research and Development Program of China (863 Program) under Grant no. 2006AA03z412, the Scientific Research Project of Hainan Education Department under Grant no. Hj 2010-52, and the Scientific Research Foundation of Graduate School of Beijing University of Chemical and Technology (no. 09Si005).

References

1. O'Regan B, Gräetzel M (1991) Nature 53:737
2. Green MA, Emery K, King D (2004) Res Appl 12:55
3. McConnell RD (2002) Renew Sustain Energy Rev 6:273
4. Fernando C, Kumarawadu I, Takahshi K (1999) Sol Energy Mater Sol Cells 58:337
5. Anpo M, Takeuchi M (2003) J Catal 216:505
6. Yin S, Yamaki H, Zhang Q, Komatsu M, Wang JS, Tang Q, Saito F, Sato T (2004) Solid State Ion 172:205

7. Asilturka M, Sayılkana F, Arpac E (2009) J Photochem Photobiol A 203:64
8. Nguyen TV, Lee HC, Khan MA, Yang OB (2007) Sol Energy 81:529
9. Choua CS, Yang RY, Weng MH, Yeh CH (2008) Adv Power Technol 19:541
10. Kawano K, Hong BC, Sakamoto K, Tsuboi T, Seo HJ (2009) Opt Mater 31:1353
11. Han ZY, Zhang JC, Yang XY, Zhu H, Cao WL (2010) J Inorg Organomet Polym Mater 20:32
12. Han ZY, Zhang JC, Yang XY, Zhu H, Cao WL (2010) Sol Energy Mater Sol Cells 94:194
13. Zeng LY, Dai SY, Wang KJ, Pan X, Shi CW, Guo L (2004) Chin Phys Lett 9:1835
14. Shi C, Yao Y, Yang Y (2006) J Am Chem Soc 128:8980
15. Sirohi S, Sharma TP (1999) Opt Mater 13:267
16. Xu ZL, Yang QJ, Xie C, Yan WJ, Du YG, Gao ZM, Zhang JH (2005) J Mater Sci 40:1539. doi:10.1007/s10853-005-0599-6
17. Han ZY, Zhang JC, Yang XY, Zhu H, Cao WL (2010) J Mater Sci Mater Electron 21:554
18. Asahi R, Morikawa T, Ohwaki T (2001) Science 293:269
19. Hagfeldt A, Gräetzel M (1995) Chem Rev 95:49
20. Kern R, Sastrawan R, Feber J (2002) Electrochim Acta 47:4213
21. Wang Q, Moser JE, Gräetzel M (2005) J Phys Chem B 109:14945